EVALUATION OF THE BALLISTIC PERFORMANCE FOR DIFFERENT COATINGS ON HARDOX 450 STEEL

Cosmin NICOLESCU[1], Marian MICULESCU[2], Tudor Viorel TIGANESCU[3]*, Ovidiu IORGA[4], Florentina ALEXE[5], Radu STEFANOIU[6], Daniela Alina NECSULESCU[7], Bogdan ISTRATE[8], Iulian ANTONIAC[9] [10]

The European defence industry depends on a wide range of materials with unique properties that make them essential for military applications. Steel is a common choice for military applications due to its durability and hardness. Hardox 450 steel is a metallic material used in vehicle armor, being considered the best compromise for high-quality requirements such as hardness, toughness, strength, and weldability. The main objective of this paper was to evaluate the ballistic strength of the Hardox 450 steel after the spray coatings with a ceramic layer (Al2O3) and a polymeric layer (polyurea), respectively. The ballistics tests were performed using different types of armament and ammunition. The bullet's velocity was measured with a ballistic chronograph, while the impact phenomena were observed using a high-speed video camera. The experimental samples were also characterized by microscopical techniques to evaluate their microstructure and coating adhesion to the substrate. The experimental results obtained demonstrated that the thermal effect of the alumina deposition process on the Hardox 450 steel plate negatively affects the Hardox 450 steel material's ballistic resistance. The polyurea coatings can provide a better ballistic protection against threats often encountered in conflict zones. The polyurea's capability to retain all the fragments resulting from impact also provides additional protection against secondary impact threats.

Keywords: steel, defense, ballistic, coatings, alumina, polyurea.

[1] PhD student, Faculty of Materials Science and Engineering, National University of Science and Technology POLITEHNICA Bucharest, e-mail: nicolescu_cosmin@yahoo.com
[2] Prof., Faculty of Materials Science and Engineering, National University of Science and Technology POLITEHNICA Bucharest, e-mail: marian.miculescu@upb.ro
[3] * Prof., Technical Science Academy Romania, Bucharest, Romania, corresponding author, e-mail: viorel.tiganescu@mta.ro,
[4] Technical Science Academy Romania, Bucharest, Romania, e-mail: iorga_ovidiu@yahoo.com
[5] Technical Science Academy Romania, Bucharest, Romania, e-mail: tiganescu.viorel.t@gmail.com
[6] Prof., Faculty of Materials Science and Engineering, National Polytechnic University of Science and Technology Bucharest, e-mail: radu.stefanoiu@upb.ro
[7] Lecturer, Faculty of Materials Science and Engineering, National University of Science and Technology POLITEHNICA Bucharest, e-mail: alina.necsulescu@upb.ro
[8] Lect., "Gheorghe Asachi" Technical University of Iasi, Faculty of Mechanical Engineering, Iasi, Romania, e-mail: bogdan.istrate@academic.tuiasi.ro
[9] Prof., Faculty of Materials Science and Engineering, National University of Science and Technology POLITEHNICA Bucharest, e-mail: antoniac.iulian@gmail.com
[10] Prof., Academy of Romanian Scientists, Bucharest, Romania

1. Introduction

The ballistic performance of military equipment - including vehicles, aircraft, and naval platforms - is critical for resisting impact and penetration. Traditionally, armor systems have been constructed from monolithic metal materials, such as steel, which, while effective in protection, often compromise mobility and operational efficiency due to their weight. This trade-off between strength and toughness in conventional metals and alloys limits their potential as stand-alone, high-performance armor materials [1,2]. Strong and flexible alloys can be made using additive manufacturing, and functional gradient materials and graphene composites offer some possibility that a single material could become protective armor to a certain extent. However, high production demands, low efficiency, easy maintenance, and fewer manufacturing process defects limit the possibility of applying the above materials on a large scale in weapons equipment in a short period [3–11].

Advanced materials like metal matrix composites and titanium alloys have been developed to address these limitations [12]. These materials exhibit excellent ballistic performance but often require increased thickness to ensure protection, thereby negatively impacting military systems' mobility and fuel efficiency. Designing high-performance armor thus requires a careful balance between weight and ballistic resistance [6].

Among protective materials, steel remains the most widely used due to its favorable mechanical properties - high strength, hardness, ductility, and formability. Its high load-bearing capacity and cost-effectiveness make it ideal for structural applications. Moreover, using thinner steel plates reduces weight without compromising structural integrity [13].

Armor's primary function is to protect against ballistic threats from firearms, anti-aircraft, and anti-tank projectiles. The increasing complexity of combat scenarios, including the use of improvised explosive devices and unconventional weaponry, has driven continuous innovation in armor systems [4].

For many military and civilian applications, protection against high-velocity projectiles is essential. Hybrid armor systems made of composite or metal coated with a hard ceramic are increasingly used to achieve ballistic protection, both for body armor and vehicle ballistic protection. The ceramic has the role of dulling and eroding the tip of the projectiles, which is usually made of a rigid material, and the coated material has the role of capturing the energy resulting from the erosion of the hard tip [5].

Coating ballistic materials with ceramics leads to armor with a lower mass than other uncoated armor that develops the same ballistic properties, thus increasing the mobility of vehicles and people. To develop ballistic materials, we must know all the mechanisms during impact. It is also essential to understand the functions of uncoated and ceramic-coated materials [5]. Ceramic coatings are

increasingly used to enhance ballistic protection. These materials - such as aluminum oxide (Al_2O_3), silicon carbide (SiC), and boron carbide (B_4C) - are valued for their high hardness, compressive strength, and low density. Coating metal substrates with ceramics like alumina significantly reduces the mass of the armor while maintaining equivalent ballistic performance, thus improving mobility. However, ceramics are brittle and can fracture under high-stress impact, which limits their standalone use. Ceramic inserts are often used in body armor to protect against armor-piercing rounds, though they can reduce comfort and flexibility [5,6].

Alumina coatings are also applied via anodizing, creating a durable aluminum oxide film that enhances corrosion and wear resistance and extends the service life of the substrate [14-16]. Despite these benefits, alumina's brittleness remains limited in dynamic impact scenarios.

Polymer materials have also gained prominence in ballistic protection, in personal armor. High-performance fibers such as Kevlar®, Twaron®, and UHMWPE (Dyneema®, Spectra®) offer high tensile strength and low weight, suitable for flexible body armor. These materials alone cannot withstand high-caliber threats, and thus, ceramic or metal plates are added for enhanced protection [17]. Kevlar has proven to be an important ballistic armor for a wide range of weapons, accessories, and ammunition. High strength, high modulus of elasticity, toughness and thermal stability are unique characteristics of Kevlar[23], [24].

In recent years, polyurea has emerged as a promising coating for ballistic applications. Known for its high impact energy absorption, elasticity, and abrasion resistance, polyurea coatings improve the shock resistance of metal substrates while maintaining a lightweight profile. Studies have demonstrated that polyurea-coated metals exhibit higher energy absorption and enhanced ballistic limits compared to uncoated counterparts. Zhang et al. [18] investigated the ballistic properties of polyurea-coated steel samples. These tests were performed by exposing the plates to impact induced by cubic-shaped fragments, and the steel samples have a low carbon composition. Polyurea was sprayed onto the sample's front side to obtain the desired ballistic properties of the plates. Using numerical methods, Liu et al. [19] examined the ballistic performance of sandwich samples (steel-polyurea-steel). The results showed that the polyurea core helps to increase the anti-penetration performance and develops self-closing behavior. Polyurea coatings are highly effective in forming waterproof barriers, making them ideal for applications where protection against water ingress is essential. These coatings are also highly flexible, allowing them to accommodate substrate movement without cracking or delaminating, thereby ensuring long-term durability [20-22]. One of the key advantages of polyurea is its rapid curing time, which enables quick project turnaround and minimizes downtime.

Furthermore, polyurea formulations can be tailored to meet specific performance requirements, such as hardness, elasticity, chemical resistance, and

abrasion resistance. Customizing these properties makes polyurea suitable for a wide range of protective applications.

2. Materials and methods

2.1. Materials used for optical microscopy and scanning electron microscopy analyses

Alumina coating was applied using the SPRAYWIZARD 9MCE plasma jet deposition system. Before coating, the metal plates were sandblasted to eliminate surface oxides, grease, and other contaminants, ensuring optimal adhesion. The coating was applied on both sides, with a layer of about 160 microns. LINE-X is a high-performance, spray-applied, two-component elastomeric system composed of 100% aromatic polyurea. It is VOC-free and consists of 100% solids, making it environmentally safe and durable. The application is carried out using a Graco Reactor E-XP2 spray machine, operating at a pressure of 150 bar, a temperature of 70 degrees Celsius, and a drying time of 10 seconds. The equipment with which LINE-X is applied is a Graco Reactor E-XP2 and a 10-bar compressed air compressor. Solvent-based degreasers, FCP primer, and LINE-X ballistic products are required in this application process. To ensure strong adhesion, it is essential to sandblast or mechanically grind the metal surface to remove rust and oxidation. The surface should be thoroughly cleaned with a solvent-based degreaser to eliminate any remaining grease or impurities. Once the primer has dried, the LINE-X protective polyurea layer is sprayed onto the surface to complete the coating process.

The experimental samples used to evaluate the microstructure and the adhesion of the coating to the substrate had a parallelepiped shape with dimensions of 15 × 15 × 10 mm. Metallographic sample preparation began with selecting a representative material specimen to accurately characterize the microstructure and relevant features. The test sample was sectioned using a Buehler Abrasimet™ Delta cutter (Buehler Ltd., Lake Bluff, IL, USA) equipped with a 102510P Buehler abrasive blade. The operation was conducted under continuous cooling to minimize mechanical deformation, which was subsequently removed during the grinding and polishing processes. The specimen was hot mounted in PhenoCure™ phenolic thermoset resin, chosen for its good edge retention and moderate shrinkage, facilitating easier handling during subsequent preparation steps. Grinding was performed using water-lubricated CarbiMet™ silicon carbide grinding papers, progressing through grit sizes from P180 to P1000. Polishing followed the Buehler SumMet method for steel, ensuring a high-quality surface finish suitable for microscopic examination. The polished samples were then etched with a 2% Nital solution to reveal the microstructure. Optical micrographs were acquired using a Nikon optical microscope (Nikon Corporation, Minato, Tokyo, Japan) with NIS-Elements software. For scanning electron microscopy (SEM) analysis, a Quanta S

STEM (Thermo Fisher Scientific Inc., Waltham, MA, USA) equipped with an energy-dispersive X-ray spectroscopy (EDS) detector was used to analyze the microstructural features in greater detail.

2.2. Materials used for the ballistic test

The ballistic testing was performed on the following structures:

- A whitness plate made of hardened steel (Hardox 450 steel) with a thickness of 5.5 mm, used as a reference;
- A composite structure consisting of a 5.5 mm Hardox 450 steel core coated on both sides with a 160 μm alumina layer (Sandwich structure alumina-steel-alumina / CHC);
- A composite structure consisting of a 5.5 mm Hardox 450 steel core coated on both sides with a 6 mm layer of LINEX X polyurea (Sandwich structure polyurea-steel-polyurea / PHP).

All ballistic tests were performed on rectangular samples measuring 250 × 250 mm. Table 1 presents each structure's specific mass.

Table 1

Types of ballistic structures tested

No.	Name of structure	Acronym	Specific mass (kg/m^2)
1	Hardox 450 steel (Whitness plate)	H	36.6
2	Sandwich alumina/steel/alumina	CHC	37.9
3	Sandwich polyurea/steel/polyurea	PHP	50.1

The ballistic tests were performed using the types of armament and ammunition mentioned in the Table 2.

Table 2

Armament systems used for ballistic testing

Ammunition type	Bullet mass	Bullet type	Armament used
7.62x54 mm API (armor piercing incendiary)	10.4 g	Copper jacket/ Steel penetrator/ incendiary composition	Semiautomatic marksman rifle PSL (Romanian version of SVD-Dragunov)
7.62x39 mm FMJ (full metal jacket)	7.9 g	Copper jacket/lead core	Automatic rifle md.1963 (Romanian version of AK-47)
5.56x45 mm NATO FMJBT (Full metal jacket boat tail)	4 g	Copper jacket/ Steel penetrator/ lead core	Hunting rifle cal. 5.56 mm
7.62x51 mm AP (armor piercing)	9.4 g	Copper jacket/ Steel penetrator	Hunting rifle Remington cal. 7.62 mm

Tests were performed in the ballistic testing range, using all the ammunition mentioned in Table 2. The rifle was placed behind a ballistic protection wall and manually actuated. The specimens were placed at the same height (1.5 m) with the rifle at 5 m away. The bullet velocity was measured using a ballistic optical barrier chronograph (HPI B462 MF), placing the optical barrier 1 m away from each other, thus achieving a 0.1 m/s measurement precision.

The specimen-bullet impact was recorded with a high-speed video camera, type Photron SA-Z, with a telescope, placed perpendicularly on the trajectory. The acquisition was set at 60000 frames per second while shutter speed was optimised in the domain 1/66000s -1/400000s. In order to illuminate the samples, 3 LED projectors were used with a 120W/1200 lumen/unit power. To avoid the glare effect on the sample's surface, a white powder spray was used to coat all the surfaces of the tested specimen (3D scan spray, Helling).

3. Results and discussion

3.1. Optical Microscopy Results

Optical microscopy images of the Hardox 450 steel before coatings, the Hardox 450 steel after alumina deposition by plasma jet deposition, and the Hardox 450 steel after LINE-X deposition were analyzed.

The optical micrographs of the uncoated sample in Fig. 1 (a and b - same area at different magnification) revealed the presence of retained austenite (light areas) with lath and plate-shaped martensite (dark areas).

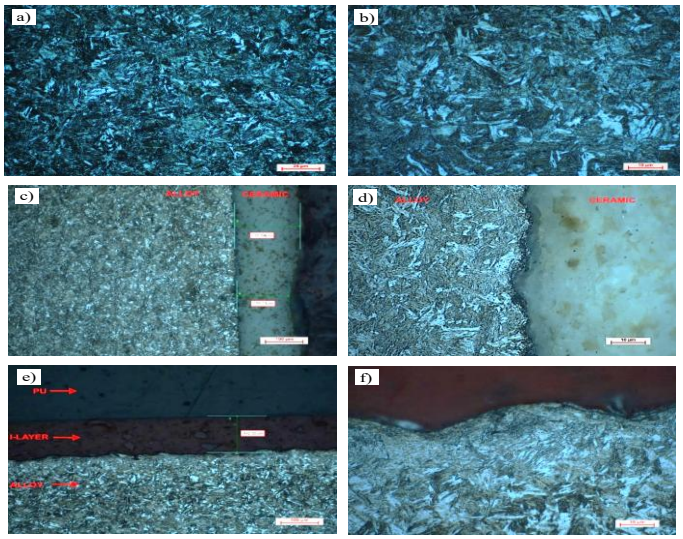

Fig. 1. Optical microscopy images of the alloy (a) and (b); alloy with alumina deposition (c) and (d); alloy with LINE-X polyurea deposition (e) and (f).

Two types of retained austenite, in blocky and film morphologies, were identified in the samples. In general, lath martensite is associated with high toughness and ductility but low strength, while plate martensite structures are much higher in strength but may be somewhat brittle and non-ductile. Martensite is very hard and brittle, while austenite is soft and rigid. In some applications, when combined, this mixture of austenite and martensite creates a material that has the

benefits of each, while compensating for the shortcomings of both, a very tough material with higher impact strength.

Figs. 1c and 1d analyze the metallic substrate and ceramic interface. Good adhesion between the two materials can be observed, and the deposited ceramic's thickness was determined to be between 140 and 180 microns. Figs. 1e and 1f show the interface between the alloy and the deposited LINE-X polyurea. An interface layer with a thickness of 140 microns is observed - the primer used before the deposition.

3.2. Results for Scanning electron microscopy coupled with EDS analysis.

Figs. 2 show the surface morphology of the Hardox 450 steel before and after the deposition of alumina and LINE-X polyurea, in cross-section area, associated with the EDS analysis performed at the interface between Hardox 450 steel substrate and coatings.

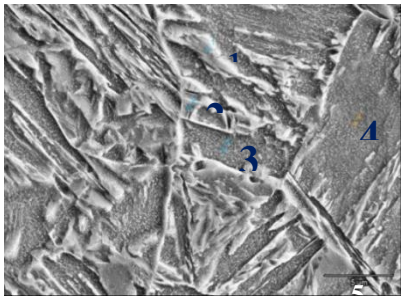

Elemental composition in the selected points obtained by EDS [wt%]

Point	C	Si	Cr	Mn	Fe	Ni	Mo
1	0.03	0.23	0.24	1.20	98.22	0.07	0.01
2	0.02	0.13	0.28	1.13	98.17	0.25	0.02
3	0.07	0.20	0.23	1.37	97.87	0.22	0.04
4	0.06	0.20	0.24	1.31	98.01	0.16	0.02

(a) Hardox 450 steel before coatings

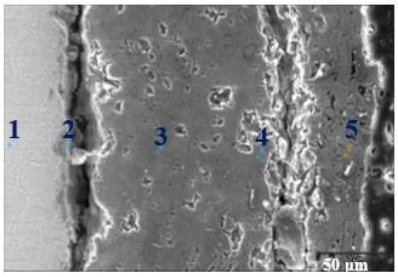

Elemental composition in the selected points obtained by EDS [wt%]

Point	C	O	Al	Si	Cr	Mn	Fe	Ni	Mo
1	0.05	0.00	0.00	0.31	0.32	1.05	98.11	0.09	0.06
2	0.11	18.89	0.00	0.00	0.04	0.16	80.80	0.00	0.00
3	0.42	30.35	36.80	0.00	0.00	0.00	32.43	0.00	0.00
4	0.44	34.83	40.16	0.00	0.00	0.00	24.57	0.00	0.00
5	0.12	31.32	46.02	0.00	0.00	0.00	22.54	0.00	0.00

(b) Hardox 450 steel after alumina deposition

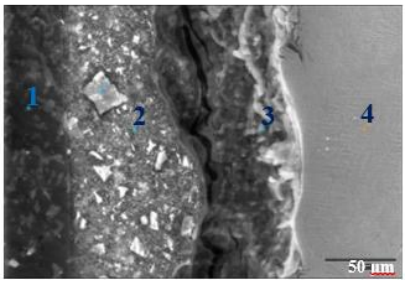

Elemental Composition in the selected points obtained by EDS [wt%]

Point	C	O	Na	Al	Si	Cr	Mn	Fe	Ni	Mo
1	68.11	28.82	0.30	0.54	0.63	0.00	0.00	1.60	0.00	0.00
2	68.84	29.02	0.15	0.97	0.82	0.00	0.00	00.20	0.00	0.00
3	0.39	23.62	0.00	0.00	0.00	0.04	0.11	75.84	0.00	0.00
4	0.50	0.00	0.00	0.00	0.51	0.28	1.21	97.36	0.06	0.08

(c) Hardox 450 steel after LINE-X polyurea deposition

Fig. 2. Surface morphology of the experimental samples in cross-section (the marked points are those for EDS analysis).

3.2.Ballistics tests

Ballistic test with 7.62x51mm AP ammunition

The ammunition is equipped with a bullet consisting of a copper jacket and a hardened steel penetrator. The bullet has a total mass of 9.4 grams and an initial velocity ≈of 850 m/s (Table 3). It has good piercing ability in light armored vehicles.

Table 3

Results after the ballistic test with 7.62x51mm AP ammunition

Test No.		Structure type	Bullet velocity (m/s)	Kinetic energy (J)	Test result
1		H	851	3403	Perforation
2		H	848	3380	Perforation
3		H	854	3427	Perforation
4		CHC	852	3411	Perforation
5		CHC	841	3324	Perforation
6		CHC	848	3379	Perforation
7		PHP	843	3340	Perforation
8		PHP	856	3444	Perforation
9		PHP	855	3403	Perforation

Table 3 shows that all types of structures were perforated each time in a three-repeated test for each type of structure. This effect is caused by the bullet's relatively high impact energy and the high stiffness of the steel penetrator used as the bullet's core.

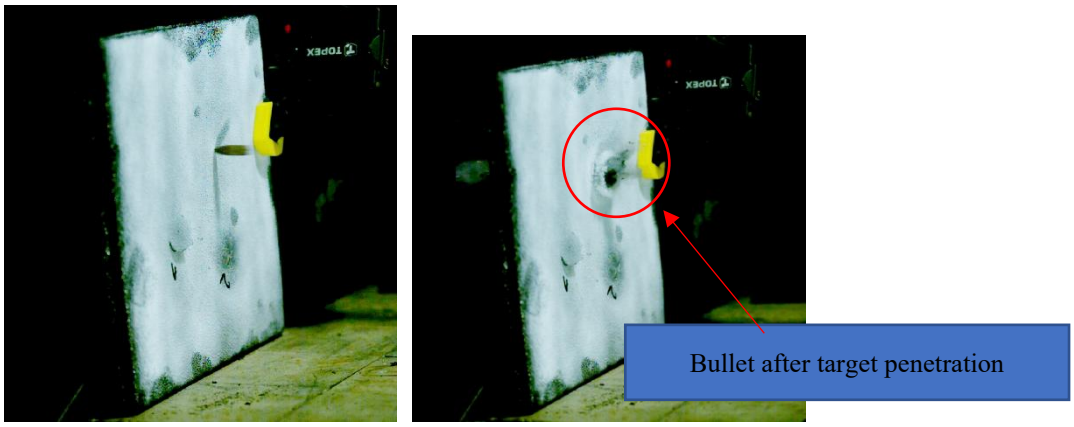

Fig. 3. The test with 7.62x51mm AP ammunition on PHP sandwich structure (Δt=250 μs between frames).

Ballistic test with 7.62x39 mm FMJ ammunition

The testing was performed with 7.62x39 mm FMJ ammunition, equipped with a general-purpose, copper jacket, lead core ammunition. The ammunition in this configuration is designed against personnel and has a limited piercing ability in hard targets. When shot with the automatic rifle, the bullet velocity is around

700m/s. The test results are presented in Table 4. When impacting the reference structure, the bullet disintegrated without causing any visible deformation on its surface. To determine the structure's ballistic resistance to this type of bullet, the velocity should have been increased by the addition of propellant powder in the ammunition cartridge. Because of security reasons, we could not increase the bullet's velocity.

Further tests on CHC și PHP sandwich structures were considered unnecessary because the reference was not perforated.

Table 4

Results after the ballistic test with 7.62x39 mm FMJ ammunition

Test No.	Structure type	Bullet velocity (m/s)	Kinetic energy (J)	Test result
1	H	685 m/s	1853 J	No perforation
2	H	692 m/s	1892 J	No perforation
3	H	696 m/s	1913 J	No perforation

Ballistic test with 5.56x45mm NATO ammunition

The ammunition is equipped with a copper jacketed bullet and a combined core, with a hardened steel perforator placed in front of a lead body. This setup makes the ammunition effective against challenging targets through its piercing capability and also against soft targets. With a bullet mass of 4g and an initial velocity of 900 m/s – 950 m/s, depending on rifle bore length, the bullet is very effective in penetrating light armor. The propellant mass could not be varied in this type of ammunition. The results of the tests are presented in Table 5, while the extracted frames from the video recorded are shown in Fig. 6.

Table 5

Test results with 5.56x45mm NATO ammunition

Test No.	Structure type	Bullet velocity (m/s)	Kinetic energy (J)	Test result
1	H	900	1620	Perforation
2	H	885	1566	Perforation
3	H	892	1591	Perforation
4	PHP	889	1581	No perforation
5	PHP	915	1674	No perforation
6	PHP	893	1595	No perforation
7	PHP	903	1631	No perforation
8	PHP	910	1656	No perforation
9	CHC	902	1627	Perforation
10	CHC	888	1577	Perforation
11	CHC	896	1606	Perforation

Test results revealed that at an initial velocity of 890 m/s—900 m/s, the bullet repeatedly (3/3) perforated the reference structure (H). Even if the bullet's

kinetic energy (≈1600 J) is lower than that of 7.62x39mm (≈1900 J), its penetration ability is greater. The use of the hardened steel penetrator in the ammunition explains this.

As observed in Fig. 4, the impact phenomenon shows the bullet's disintegration. The side copper jacket and the lead core are dispersed radially (Fig. 4 d-h), while the steel penetrator and the tip of the copper jacket penetrate the target and split behind the plate in two distinct parts (Fig. 4 e-l).

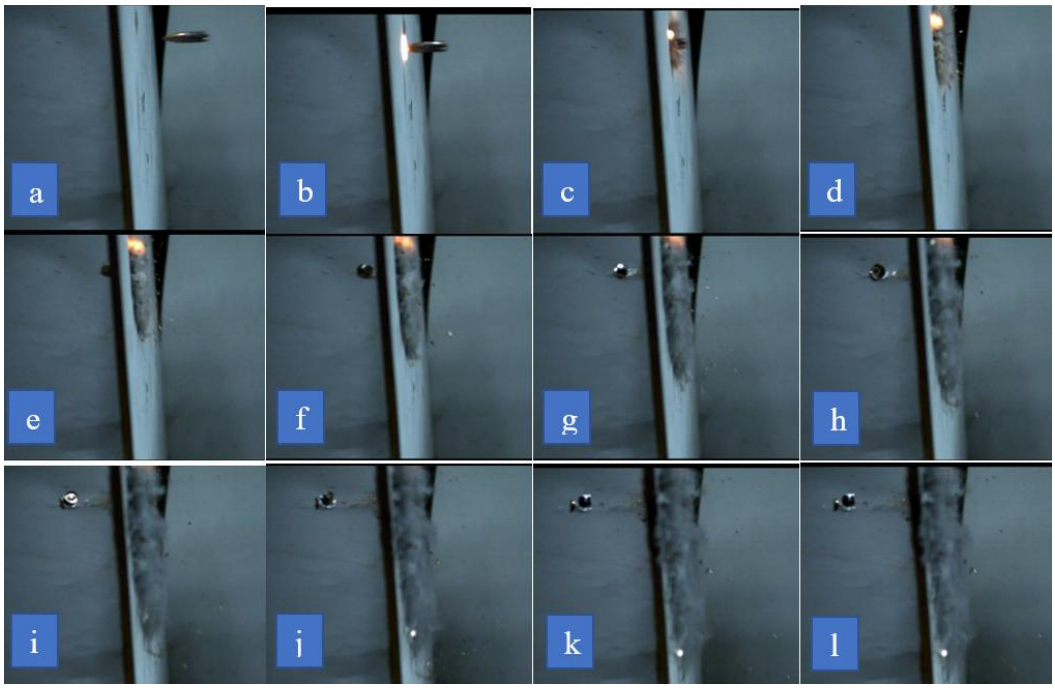

Fig. 4. Perforation of reference structure (H) by a 5.56x45mm NATO bullet with a velocity of 885 m/s. Total duration of the presented sequence 166 μs, Δt=16 μs between frames.

In comparison, the PHP sandwich structure withstands impacts (5/5 tests) to the same type of bullet, with velocity ranging from 890m/s to 915m/s, fully retained in the front layer of polyurethane. Fig. 5 shows a sequence of frames extracted from the impact recording between a 5.56x45 mm NATO bullet with 910m/s and a PHP structure. From the recordings, we observe the formation of a temporary bubble (forming at about 200μs after impact and collapsing in about 500 μs). Also, the whole structure is buckling, which means the energy is transferred and dissipated to the ballistic protection structure.

We can also observe an excellent capacity to retain all the debris and fragments from bullet desintegration inside the formed bubble. This property of the structure is significant in ballistic protection, as it prevents casualties from wounds caused by fragments.

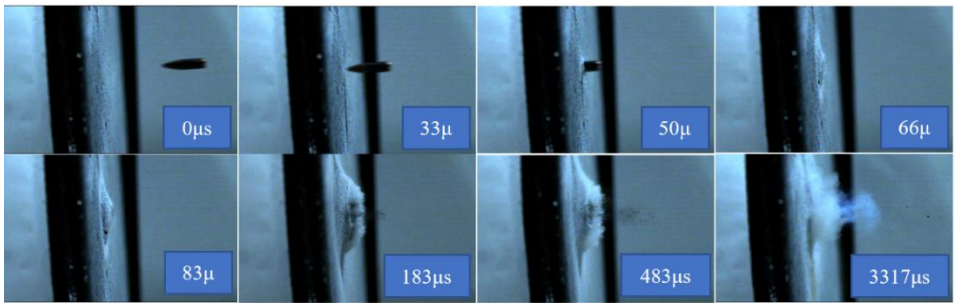

Fig. 5. Impact between a 910m/s velocity 5.56x45mm NATO bullet and the PHP sandwich structure.

When testing the sandwich structure CHC (Alumina/Hardox plate/Alumina), we observed no improvement in ballistic protection compared to the reference structure (H). When impacting the structure with a 5.56x45mm NATO bullet with a velocity of 902 m/s, we observe rapid delamination of both layers of alumina deposited in the Hardox 450 steel plate, as shown in Figs. 6-7.

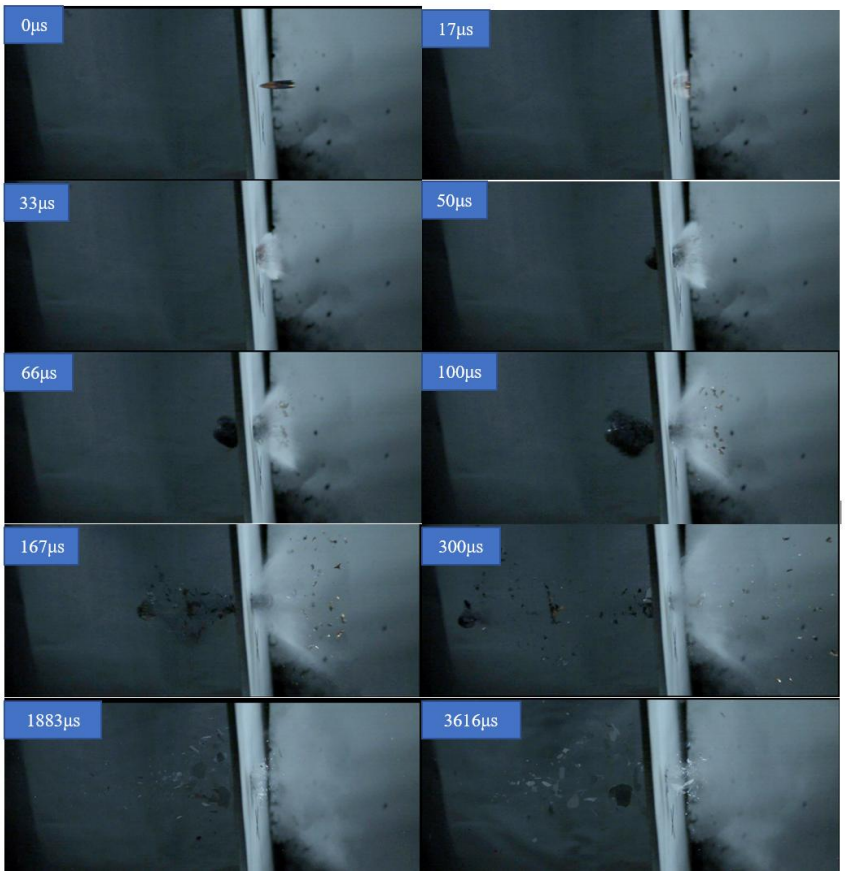

Fig. 6. Impact between a 902 m/s velocity 5.56x45mm NATO bullet and the CHC sandwich structure.

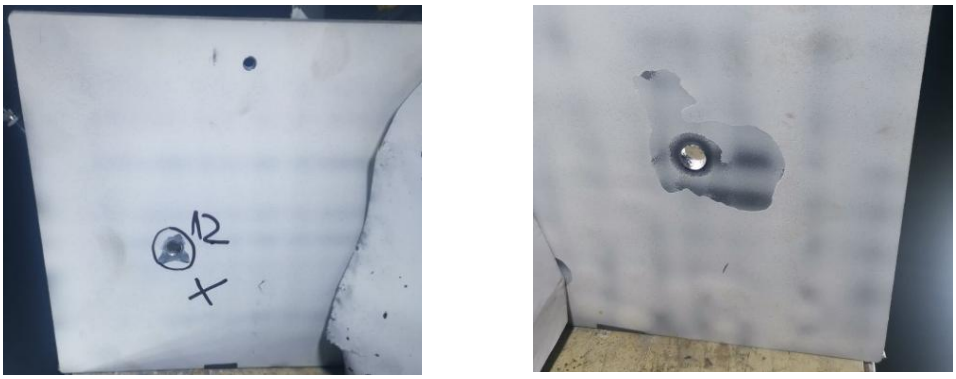

(a) frontal area (b) backside area

Fig. 7. Alumina delamination in the impact zone, the perforation produced by a 5.56x45mm NATO bullet

Surprisingly, after impact examination, it was evident that the diameter of bullet penetration in the CHC structure is larger than the diameter of the bullet penetration in reference plate H. This could mean that the Hardox 450 steel suffered the loss of resistance induced by the thermal effect of alumina deposition. This aspect is illustrated in Fig. 8.

Fig. 8. The perforation produced by a 5.56x45mm NATO bullet to the reference plate (H)-left and to the CHC sandwich -right.

Ballistic test with 7.62x54 API ammunition

This type of ammunition is API armor piercing incendiary and is fired with a marksman rifle or machine gun. The initial velocity of the bullet is around 809 m/s. The bullet configuration is designed to perforate 7 mm homogeneous armor steel material at 200 m in 8/10 trials. Additionally, the bullet also has an incendiary effect. On this type of ammunition, we could lower the propellant mass to vary the bullet velocity within the scope of determining the ballistic limit of each type of structure. The results of the tests are shown in Table 6.

Table 6

Test results with 7.62x54 mm API ammunition

Test No.	Structure type	Bullet velocity (m/s)	Kinetic energy (J)	Test result
1	H	864	3882	Perforation
2	H	712	2636	Perforation
3	H	634	2090	Perforation
4	H	567	1672	Perforation
5	H	550	1573	Perforation
6	H	536	1494	Perforation
7	H	521	1411	No perforation
8	H	514	1374	No perforation
9	H	507	1337	No perforation
10	CHC	591	1816	Perforation
11	CHC	540	1516	Perforation
12	CHC	518	1395	Perforation
13	CHC	473	1163	Perforation
14	CHC	448	1044	Perforation
15	PHP	865	3891	Perforation
16	PHP	722	2711	Perforation
17	PHP	700	2548	Perforation
18	PHP	691	2483	No perforation
19	PHP	689	2469	No perforation
20	PHP	687	2454	No perforation

As it can be observed, the impact of the API projectile at nominal velocity produces total perforation in all types of structures. In Fig. 9, the incendiary effect can also be observed. The bullet doesn't suffer considerable deformation and is not diverted from the trajectory. This means that the ballistic limit of the tested structures is much lower when subjected to the impact of an API bullet with considerable mass, like this one. Further, we lowered the bullet velocity until we observed that the tested structure are not perforated.

At this limit, we performed another 2 confirmatory tests at similar velocities. In the case of the CHC structure, the ballistic limit could not be determined because the structure was penetrated even at 1044 J energy. We could determine a ballistic limit of PHP structure 2483 J, while the ballistic limit for the reference structure, Hardox 450 steel plate, was determined to be 1337 J.

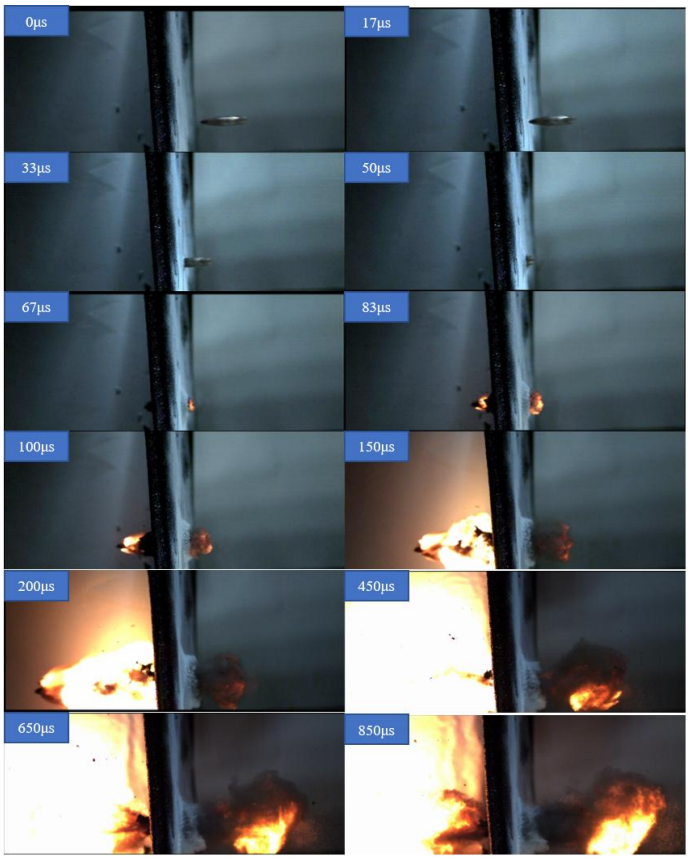

Fig. 9. Impact of PHP structure with a 7.62x54 mm API bullet with 865 m/s velocity.

When comparing the results with the specific mass of the structure, we can observe a substantial ballistic improvement in the case of PHP (+76% more energy) while the mass is increased by only 37%.

4. Conclusions

The thermal effect of the alumina deposition process on the Hardox 450 steel plate negatively affects the ballistic resistance of the Hardox 450 steel, due to the microstructural modification induced by the heating during deposition process. This can be observed from the tests performed with 5.56x45 mm NATO and 7.62x54 mm API ammunition.

The PHP sandwich structure can provide ballistic protection against threats often encountered in conflict zones (7.62x39 mm FMJ and 5.56x45 mm NATO armor piercing). This means that the layers of polyurea could be coated directly on both sides of a light armored vehicle, thus considerably raising its ballistic protection ability.

The PHP sandwich structure, compared with the used reference plate (Hardox steel), proved a substantial ballistic protection improvement when exposed to armor-piercing projectiles in terms of kinetic energy (76%) while the specific mass was raised by only 36%. The polyurea's capability to retain all the fragments resulting from impact also provides additional protection against secondary impact threats.

REFERENCES

[1]. *Wang, Y.; Chen, M.; Zhou, F.; Ma, E.* High Tensile Ductility in a Nanostructured Metal. Nature 2002, **419**, 912–915, doi:10.1038/nature01133.

[2]. *Fang, T.H.; Li, W.L.; Tao, N.R.; Lu, K*. Revealing Extraordinary Intrinsic Tensile Plasticity in Gradient Nano-Grained Copper. Science 2011, **331**, 1587–1590, doi:10.1126/science.1200177.

[3]. *Wang, Y.M.; Voisin, T.; McKeown, J.T.; Ye, J.; Calta, N.P.; Li, Z.; Zeng, Z.; Zhang, Y.; Chen, W.; Roehling, T.T.*; et al. Additively Manufactured Hierarchical Stainless Steels with High Strength and Ductility. Nature Mater 2018, **17**, 63–71, doi:10.1038/nmat5021.

[4]. *Hu, P.; Cheng, Y.; Zhang, P.; Liu, J.; Yang, H.; Chen, J. A* Metal/UHMWPE/SiC Multi-Layered Composite Armor against Ballistic Impact of Flat-Nosed Projectile. Ceramics International 2021, **47**, 22497–22513, doi:10.1016/j.ceramint.2021.04.259.

[5]. *Ren, J.; Zhang, Y.; Zhao, D.; Chen, Y.; Guan, S.; Liu, Y.; Liu, L.; Peng, S.; Kong, F.; Poplawsky, J.D.*; et al. Strong yet Ductile Nanolamellar High-Entropy Alloys by Additive Manufacturing. Nature 2022, **608**, 62–68, doi:10.1038/s41586-022-04914-8.

[6]. *Huang, Y.; Wan, C.* Controllable Fabrication and Multifunctional Applications of Graphene/Ceramic Composites. J Adv Ceram 2020, **9**, 271–291, doi:10.1007/s40145-020-0376-7.

[7]. *Boldin, M.S.; Berendeev, N.N.; Melekhin, N.V.; Popov, A.A.; Nokhrin, A.V.; Chuvildeev, V.N.* Review of Ballistic Performance of Alumina: Comparison of Alumina with Silicon Carbide and Boron Carbide. Ceramics International 2021, **47,** 25201–25213, doi:10.1016/j.ceramint.2021.06.066.

[8]. *Dresch, A.B.; Venturini, J.; Arcaro, S.; Montedo, O.R.K.; Bergmann, C.P*. Ballistic Ceramics and Analysis of Their Mechanical Properties for Armour Applications: A Review. Ceramics International 2021, **47**, 8743–8761, doi:10.1016/j.ceramint.2020.12.095.

[9]. *Bowen, J.J.; Mooraj, S.; Goodman, J.A.; Peng, S.; Street, D.P.; Roman-Manso, B.; Davidson, E.C.; Martin, K.L.; Rueschhoff, L.M.; Schiffres, S.N.*; et al. Hierarchically Porous Ceramics via Direct Writing of Preceramic Polymer-Triblock Copolymer Inks. Materials Today 2022, **58**, 71–79, doi:10.1016/j.mattod.2022.07.002.

[10]. *Marx, J.; Rabiei, A.* Overview of Composite Metal Foams and Their Properties and Performance. Advanced Engineering Materials 2017, **19**, 1600776, doi:10.1002/adem.201600776.

[11]. *Umanzor, M.E.; Batra, R.C.; Williams, C.B.; Druschitz, A.P*. Penetration Resistance of Cast Metal−Ceramic Composite Lattice Structures. Advanced Engineering Materials 2021, **23**, 2100577, doi:10.1002/adem.202100577.+

[12]. *Matei, AA; Pencea, I; Stanciu, GA* et al. Structural characterization and adhesion appraisal of TiN and TiCN coatings deposited by CAE-PVD technique on a new carbide composite cutting tool. Journal of Adhesion Science and Technology 2015, **29**, 2576-2589, doi.org/10.1080/01694243.2015.1075857

[13]. *Børvik, T.; Dey, S.; Clausen, A.H.* Perforation Resistance of Five Different High-Strength Steel

Plates Subjected to Small-Arms Projectiles. International Journal of Impact Engineering 2009, **36**, 948–964, doi:10.1016/j.ijimpeng.2008.12.003.

[14]. *Istrate, B; Rau, JV; Saceleanu, V* et al. Properties and in vitro assessment of ZrO2-based coatings obtained by atmospheric plasma jet spraying on biodegradable Mg-Ca and Mg-Ca-Zr alloys. Ceramics International 2020, **46** (10), 15897-15906, doi:10.1016/j.ceramint.2020.03.138

[15]. *Krishnan, S.V.; Ambalam, M.M.; Venkatesan, R.; Mayandi, J.; Venkatachalapathy, V.* Technical Review: Improvement of Mechanical Properties and Suitability towards Armor Applications – Alumina Composites. Ceramics International 2021, **47**, 23693–23701, doi:10.1016/j.ceramint.2021.05.146.

[16]. *Antoniac, IV; Stoia, DI; Saceleanu, V* et al. Failure Analysis of a Humeral Shaft Locking Compression Plate Surface Investigation and Simulation by Finite Element Method. Materials 2019, **12** (7), doi:10.3390/ma12071128

[17]. *Rashid, A.B.; Hoque, M.E.* 14 - Polymer Nanocomposites for Defense Applications. In Advanced Polymer Nanocomposites; Hoque, M.E., Ramar, K., Sharif, A., Eds.; Woodhead Publishing in Materials; Woodhead Publishing, 2022; 373–414 ISBN 978-0-12-824492-0.

[18]. *Zhang, P; Wang, Z; Zhao, P; Zhang, L; Jin, X.C; Xu, Y*.Experimental investigation on ballistic resistance of polyurea coated steel plates subjected to fragment impact. Thin-Walled Structures 2019, **144**, 106342, doi:10.1016/j.tws.2019.106342

[19]. *Liu, Q.Q; Wang, S.P; Lin, X; Cui, P; Zhang, S*. Numerical simulation on the anti-penetration performance of polyurea-core Weldox 460 E steel sandwich plates. Composite Structures 2020, **236**, 111852, doi:10.1016/j.compstruct.2019.111852

[20]. *Si, P.; Liu, Y.; Yan, J.; Bai, F.; Shi, Z.; Huang, F*. Effect of Polyurea Layer on Ballistic Behavior of Ceramic/Metal Armor. Structures 2023, **48**, 1856–1867, doi:10.1016/j.istruc.2023.01.089.

[21]. *Mohotti, D.; Ngo, T.; Mendis, P.; Raman, S.N.* Polyurea Coated Composite Aluminium Plates Subjected to High Velocity Projectile Impact. Materials & Design (1980-2015) 2013, **52**, 1–16, doi:10.1016/j.matdes.2013.05.060.

[22]. *Luo, B.* Effect of Polyurea Interlayer on Ballistic Performance of Ceramic Armor Module against Long Rod Impact. 2020, doi:10.32657/10356/145914.

[23]. *DuPoint*, Kevlar Aramid Fiber - Technical Guide.

[24]. *E. G. Chatzi & J. L. Koenig* , „ Morphology and Structure of Kevlar Fiber: A review," Polymer-Plastics Technology and Engineering, 1989.